ELSEVIER

15 September 1995

Optics Communications 119 (1995) 491–498

OPTICS COMMUNICATIONS

Tunable axial superresolution by annular binary filters. Application to confocal microscopy

Manuel Martínez-Corral [a], Pedro Andrés [a], Jorge Ojeda-Castañeda [b], Genaro Saavedra [a]

[a] *Departamento de Optica, Universidad de Valencia, 46100 Burjassot, Spain*

[b] *Instituto Nacional de Astrofísica, Optica y Electrónica, Apartado Postal 216, Puebla 72000, Puebla, Mexico*

Received 10 May 1995

Abstract

We present a set of annular binary pupil filters for increasing the axial resolving capacity of imaging systems. The filters consist of two transparent annuli of the same area. It is shown that by changing the area of the transparent regions it is possible to obtain a tunable reduction of the width of the central lobe of the axial point spread function of the imaging system. However, this reduction is accompanied by a severe increase of the strength of secondary lobes, what can make these filters not very useful when used in conventional imaging systems. That is why we propose to use these filters for apodizing confocal microscopy systems. It is shown that in this case an important reduction is achieved in the volume of the central lobe of the three-dimensional point spread function.

1. Introduction

The intensity distribution in the three-dimensional (3D) image of a point source provided by an imaging system, i.e., the intensity point spread function (PSF) of the system, is governed by the finite extent and the amplitude transmission of the exit pupil as well as the wavelength of the radiation. Several efforts have been addressed to modify the characteristics of this PSF in order to improve the quality of the image. In this sense, the use of nonuniform transmission filters to produce apodization [1,2] or superresolution [1–4] on the transverse intensity PSF, i.e., on the intensity distribution at the image plane, is well known.

More recently, the effects of nonuniform transmission filters in the axial PSF have been studied. In this sense, certain filters have been proposed for achieving a high focal depth [5,6], for reducing the influence of spherical aberrations [7], for obtaining zero-axial irradiance for optical alignment [8], or even for removing the energy from the axial point of the image plane with the aim of achieving high precision focusing [9].

The design of filters for achieving superresolution along the optical axis is of great importance in 3D imaging because the narrower the central lobe of the axial response, the higher the optical-sectioning capacity of the system. However, not too much attention has been paid to the design of this kind of filters [10,11].

The aim of this paper is to design a set of annular binary filters for increasing at will the axial resolution capacity of imaging systems. The binary filters are composed by two transparent annuli of the same area, and we show that the lower the area of the annuli, the narrower the width of the central lobe of the axial intensity PSF. The use of these filters permits to reduce the width of the central lobe of the axial intensity PSF up to a factor 1/2. In the limit cases, this reduction is accompanied by a big enlargement of secondary lobes,

SSDI 0030-4018(95)00380-0

which can be detrimental in conventional imaging. We also prove that the use of these filters does not affect, up to the second-order approximation, the width of the central lobe of the transverse intensity PSF.

In a second step we propose to use the above filters for improving the imaging properties of confocal microscopes. Several proposals have been made in order to modify the intensity PSF of such systems [12–18]. In this context we show that the use of the proposed annular binary filters permits to obtain a drastic improvement of the sectioning capacity of the system, while keeping the transverse resolution.

In Section 2, we discuss the influence of the pupil filter transmittance on the transverse and axial superresolving capacity of an imaging system. In Section 3, we apply the previous formalism to design a set of binary filters for achieving axial superresolution. Finally, in Section 4 we show that the use of these filters in a confocal microscopy system permits to reduce the volume of the central lobe of the 3D intensity PSF.

2. Basic theory

Let us start by considering the amplitude PSF, $p(v, W_{20})$, of an aberration-free imaging system that is apodized by a radially-symmetric pupil function $\tilde{p}(\rho)$, ρ being the normalized radial coordinate. For this case

$$p(v, W_{20}) = 2\int_0^1 \tilde{p}(\rho)\exp(-i2\pi W_{20}\rho^2) \times J_0(2\pi v\rho)\rho\,d\rho\,. \quad (1)$$

In Eq. (1), $v = r_0 r/\lambda f$ stands for the radial variation in the image volume, r_0 being the maximum radial extent of the pupil and f the focal length of the system, whereas W_{20} specifies the amount of defocus measured in units of wavelength. Finally, J_0 denotes the Bessel function of the first kind and zero order.

Next, we particularize Eq. (1) for two cases of special interest: the amplitude distribution along the optical axis, and at the image plane. For the optical axis we set $v = 0$ in Eq. (1) to give

$$p(0, W_{20}) = 2\int_0^1 \tilde{p}(\rho)\exp(-i2\pi W_{20}\rho^2)\rho\,d\rho\,. \quad (2)$$

Now, it is possible to convert Eq. (2) into a one-dimensional (1D) Fourier transform by using the next geometrical mapping:

$$\zeta = \rho^2 - 0.5, \quad q(\zeta) = \tilde{p}(\rho)\,. \quad (3)$$

If we substitute Eq. (3) into Eq. (2), then we have that, except for an irrelevant phase factor, the axial amplitude PSF can be described by

$$p(0, W_{20}) = \int_{-0.5}^{0.5} q(\zeta)\exp(-i2\pi W_{20}\zeta)\,d\zeta\,. \quad (4)$$

It is apparent from Eq. (4) that the complex-amplitude distribution along the optical axis is related with the mapped amplitude transmittance of the pupil, $q(\zeta)$, by a 1D Fourier transformation.

On the other hand, for the image plane case, $W_{20} = 0$, we have that

$$p(v, 0) = 2\int_0^1 \tilde{p}(\rho)J_0(2\pi v\rho)\rho\,d\rho\,. \quad (5)$$

Then, the two-dimensional (2D) amplitude distribution in the image plane is given by the Hankel transform of zero order of the apodizing function. The geometrical transformation of Eq. (3) can also be applied to Eq. (5). In this case, the transverse amplitude PSF can be rewritten as

$$p(v, 0) = \int_{-0.5}^{0.5} q(\zeta)J_0(2\pi v\sqrt{\zeta + 0.5})\,d\zeta\,. \quad (6)$$

Now, we can state that both the transverse and the axial amplitude PSF of an apodized imaging system are governed by the same function, $q(\zeta)$, but through two different types of transformation.

As we are interested in the design of filters for increasing the resolving capacity of an optical system along the optical axis, but taking also into account the effects in the transverse plane, it is convenient to introduce the axial and transverse resolution gains defined by Sheppard and Hegedus [11], which evaluate the fall-off in intensity in the focal region of an apodized imaging system in comparison with that corresponding to a nonapodized one.

Following a reasoning similar to that of Ref. [11] (see appendix), we obtain from Eqs. (4) and (6) that,

within the second-order approximation, the variation of the normalized intensity in the focal region of an apodized system is given by:
(a) the image plane, see Eq. (A.8),

$$I_N(v,0)=\frac{I(v,0)}{I(0,0)}=1-\pi^2\left(1+2\frac{m_1}{m_0}\right)v^2=1-\pi^2(1+2\bar{\zeta})v^2\,, \tag{7}$$

(b) the optical axis, see Eq. (A.4),

$$I_N(0,W_{20})=\frac{I(0,W_{20})}{I(0,0)}=1-4\pi^2\left[\left(\frac{m_1}{m_0}\right)^2-\frac{m_2}{m_0}\right]W_{20}^2=1-4\pi^2\sigma^2W_{20}^2\,. \tag{8}$$

In Eqs. (7) and (8), the coefficient

$$m_n=\int_{-0.5}^{0.5}q(\zeta)\zeta^n\mathrm{d}\zeta\,,\quad n=0,1,2\,, \tag{9}$$

represents the nth moment of $q(\zeta)$, $\bar{\zeta}$ is the mean abscissa, and σ the standard derivation.

Then, the transverse, G_T, and the axial, G_A, resolution gains, with respect to the second-order intensity fall-off corresponding the clear circular aperture, may be defined as

$$G_T=\sqrt{\frac{1+2\bar{\zeta}_a}{1+2\bar{\zeta}_c}}\,, \tag{10a}$$

$$G_A=\frac{\sigma_a}{\sigma_c}\,, \tag{10b}$$

where subscript c corresponds to the nonapodized circular pupil, whereas subscript a corresponds to the apodized pupil.

The merit functions defined in Eqs. (10) represent the ratio between the width of the second-order intensity fall-off provided by the nonapodized circular aperture and that provided by the apodized one. Therefore, when a superresolving effect is achieved in one of both directions, transverse or axial, the value of the corresponding gain is bigger than unity. In the opposite case, the gain is smaller than unity. Thus, it is apparent from these equations that an axial superresolving effect is obtained when $\sigma_a>\sigma_c$, whereas for obtaining transverse superresolution it is necessary that $\bar{\zeta}_a>\bar{\zeta}_c$.

For the clear circular pupil, $q(\zeta)=1$, the value of the moments are

$$m_0=1,\quad m_1=0,\quad \text{and}\quad m_2=1/12\,. \tag{11a}$$

So, the values of the mean abscissa and the standard deviation are, respectively,

$$\bar{\zeta}_c=0\,,\quad \text{and}\quad \sigma_c=\sqrt{1/12}\,. \tag{11b}$$

Thus, the transverse and axial gains can be rewritten as

$$G_T=\sqrt{1+2\bar{\zeta}_a}\,,\quad \text{and}\quad G_A=\sqrt{12}\sigma_a\,. \tag{12}$$

The merit functions in Eq. (12) are equivalent to those defined by Sheppard and Hegedus, except for a square root operation.

Finally, we would like to highlight that, aside from minor details, the above developed basic theory is fully based on Ref. [11].

3. Annular binary filters design

As it is pointed out in Section 2, for obtaining an axial superresolving effect, we need that the standard deviation of the mapped function of the apodized pupil is bigger than that corresponding to the nonapodized circular aperture. Then, it is clear that this effect can be achieved by a radially-symmetric pupil filter provided that the value of its corresponding mapped function, $q(\zeta)$, in the vicinity of $\zeta=-0.5$ and $\zeta=+0.5$ is much bigger than at $\zeta=0$. These conditions are fulfilled by a wide set of pupil functions as, for example, that characterized by the mapped function $q(\zeta)=4\zeta^2$, which corresponds under the geometrical mapping of Eq. (3) to the well-known radially-symmetric pupil filter of the form $\tilde{p}(\rho)=4\rho^4-4\rho^2+1$ [11,19]. However, the practical implementation of such a type of purely absorbing filters, in which the amplitude transmittance varies as a monotonic function of the radial coordinate, is not an easy task. One way to face this question is to develop and optimize the binarization method which better suits our apodization problem [12,20,21].

These difficulties can be overcome by designing filters whose amplitude transmittance is binary. According to this requirement, we propose the set of annular

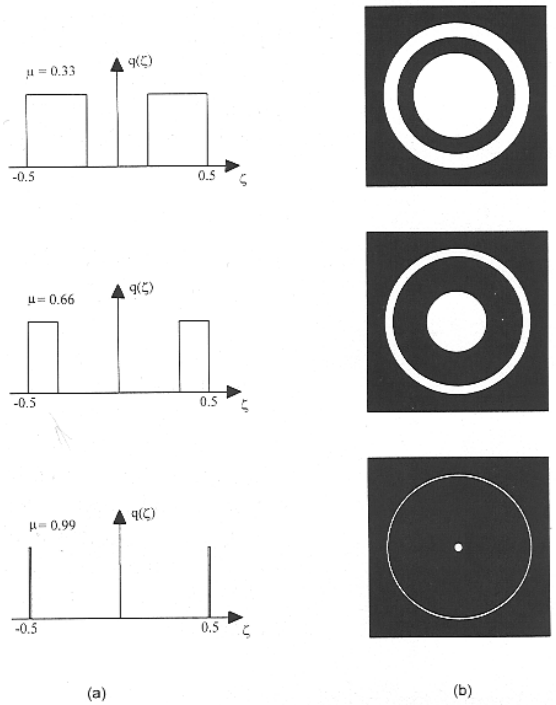

Fig. 1. Three members of the family of axially superresolving pupil filters of Eq. (13): (a) mapped function $q(\zeta)$ for $\mu = 0.33, 0.66$, and 0.99; (b) actual 2D representation.

binary filters characterized by the mapped function

$$q(\zeta) = \mathrm{rect}(\zeta) - \mathrm{rect}(\zeta/\mu)\ ,\ \text{with}\ 0 < \mu < 1\ . \qquad (13)$$

Any member of the above family of filters consists of a circular aperture obstructed by an annular mask, in such way that the two transparent annuli of the filter have the same area. This fact is illustrated in Fig. 1, where we have represented, for three different values of the obscuration-ratio parameter μ, the function $q(\zeta)$ and its corresponding 2D version $\tilde{p}(\rho)$.

The on-axis intensity distribution, $I(0, W_{20}) = |p(0, W_{20})|^2$, generated by these filters is given by the square modulus of the 1D Fourier integral of Eq. (4), i.e.,

$$I(0, W_{20}) = |\mathrm{sinc}(W_{20}) - \mu\,\mathrm{sinc}(\mu W_{20})|^2\ . \qquad (14)$$

In Fig. 2 we have represented, by dashed curves, the normalized version of Eq. (14), $I_N(0, W_{20}) = I(0, W_{20})/I(0,0)$, corresponding to the filters shown in Fig. 1. For comparison, the axial intensity PSF corresponding to the nonapodized circular pupil (CP), is also plotted (solid curve).

From Figs. 1 and 2 it is quite apparent that as the value of the parameter μ increases, the area of the transparent annuli of the filter decreases and the central lobe of the normalized axial intensity distribution gradually narrows. In the limit case, in which the value of μ approaches unity, the filter consists on an infinitely narrow annulus and a pinhole, and it provides the maximum axial resolution attainable with purely absorbing pupil filters. Note that this set of binary filters reproduces, in a certain way, the Young experiment, but along the optical axis, and permits, by a continuous variation of parameter μ, to control between certain limits the axial resolution of the system.

In order to investigate the superresolving properties of the proposed filters, not only along the optical axis but also in the image plane, we may use the axial and transverse resolution gains defined in Eq. (12). For this purpose, we first calculate the different moments of our annular binary filters. We obtain

$$m_0 = 1 - \mu\ ,\quad m_1 = 0\ ,\quad \text{and}\quad m_2 = (1 - \mu^3)/12\ , \qquad (15a)$$

and then the beam abscissa and the standard deviation are

$$\bar{\zeta}_a = 0\ ,\quad \text{and}\quad \sigma_a = \sqrt{(\mu^2 + \mu + 1)/12}\ , \qquad (15b)$$

respectively. Therefore, the transverse and the axial resolution gains provided by our annular binary filters are, respectively,

$$G_T = 1\ ,\quad \text{and}\quad G_A = \sqrt{\mu^2 + \mu + 1}\ . \qquad (16)$$

In Fig. 3, we have plotted the variation of both gain coefficients as a function of the parameter μ. It is appar-

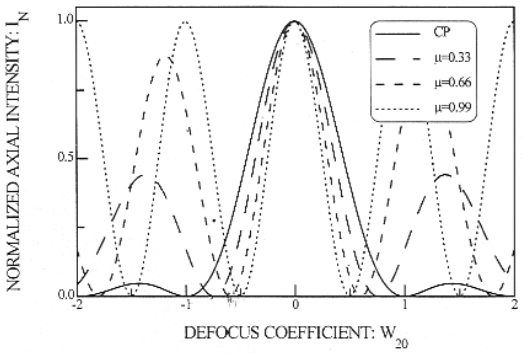

Fig. 2. Normalized axial intensity PSF for the filters in Fig. 1 and for the nonapodized circular pupil (CP).

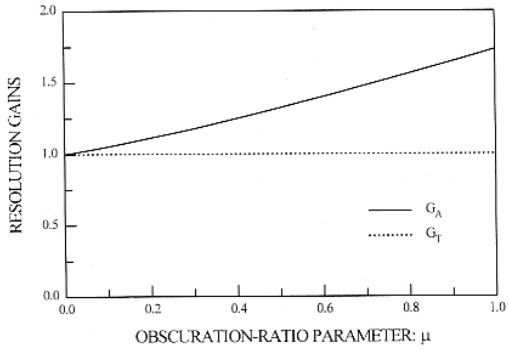

Fig. 3. Transverse, G_T, and axial, G_A, resolution gain versus the obscuration-ratio parameter μ.

ent from this figure that, within the second-order approximation, the transverse resolution of a system apodized by one of our filters remains unchanged, i.e., the central lobe of the transverse PSF does not spread. In fact, any pupil filter represented by an even mapped function is neutral in the transverse direction [11]. On the contrary, the axial resolution gradually increase as the parameter μ approaches unity.

The combination of both results allows us to recognize that the use of these annular binary filters permits to obtain a 3D PSF in which the area of the central lobe can be gradually decreased. Thus, in this sense, it can be stated that these filters have the ability of increasing the 3D resolution of an optical system or, equivalently, that they provide a 3D superresolution effect.

4. Application to confocal microscopy

The use of the proposed filters for increasing the axial resolution of a conventional imaging system presents certain drawbacks. On the one hand, because of the introduction of an annular stop , part of the energy is obstructed providing a light throughput much lower than with a circular pupil. At the same time, the narrowness of the central lobe of the axial PSF is accompanied by a severe increasing of the strength of the secondary lobes. These drawbacks can make these filters not very useful when used in conventional imaging systems.

However, if a confocal scanning microscope architecture is used [22], these collateral effects are overcome to a certain extent. The principle of the confocal scanning microscope is schematically illustrated in Fig. 4. In this setup, the light from a point source probes a small region of the object. Then, the transmitted light is collected and focused onto a point detector. Here, the 3D intensity PSF of the system depends on the properties of both the illuminating and the collecting system, and it is given by [23]

$$I(v, W_{20}) = |p_1(v, W_{20}) p_2(v, W_{20})|^2 , \qquad (17)$$

where $p_1(v, W_{20})$ and $p_2(v, W_{20})$ are the amplitude PSFs corresponding to the pupil functions $\tilde{p}_1$ and $\tilde{p}_2$, respectively (see Fig. 4).

From Eq. (17) it is clear that the intensity PSF is given by the product of two independent functions. This multiplicative character can be exploited for reducing the collateral effects of our superresolving filters. This is achieved by combining one of these filters, used for example as the collecting system pupil, and a clear circular aperture, used as the illuminating-system pupil.

In this case, the secondary lobes of the axial PSF of the superresolving filter, $p_2(0, W_{20})$, are drastically reduced when multiplied by the axial PSF of the cir-

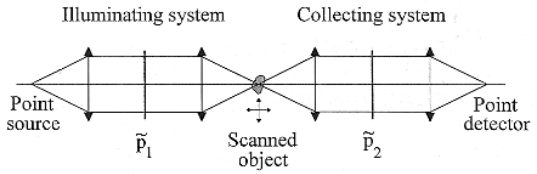

Fig. 4. Scheme of a confocal imaging system.

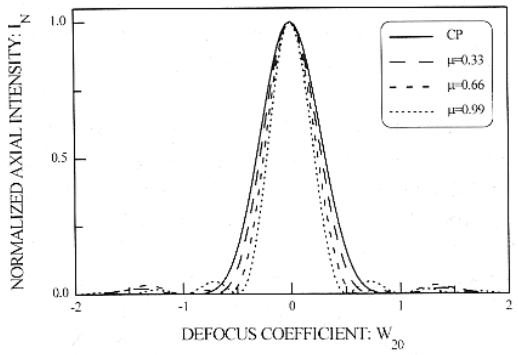

Fig. 5. Normalized axial intensity PSF of a confocal microscope whose collecting system incorporates one of the filters depicted in Fig. 1. The solid curve corresponds to the nonapodized system. In this plot we assume that both illuminating and collecting pupils have the same outermost radius,

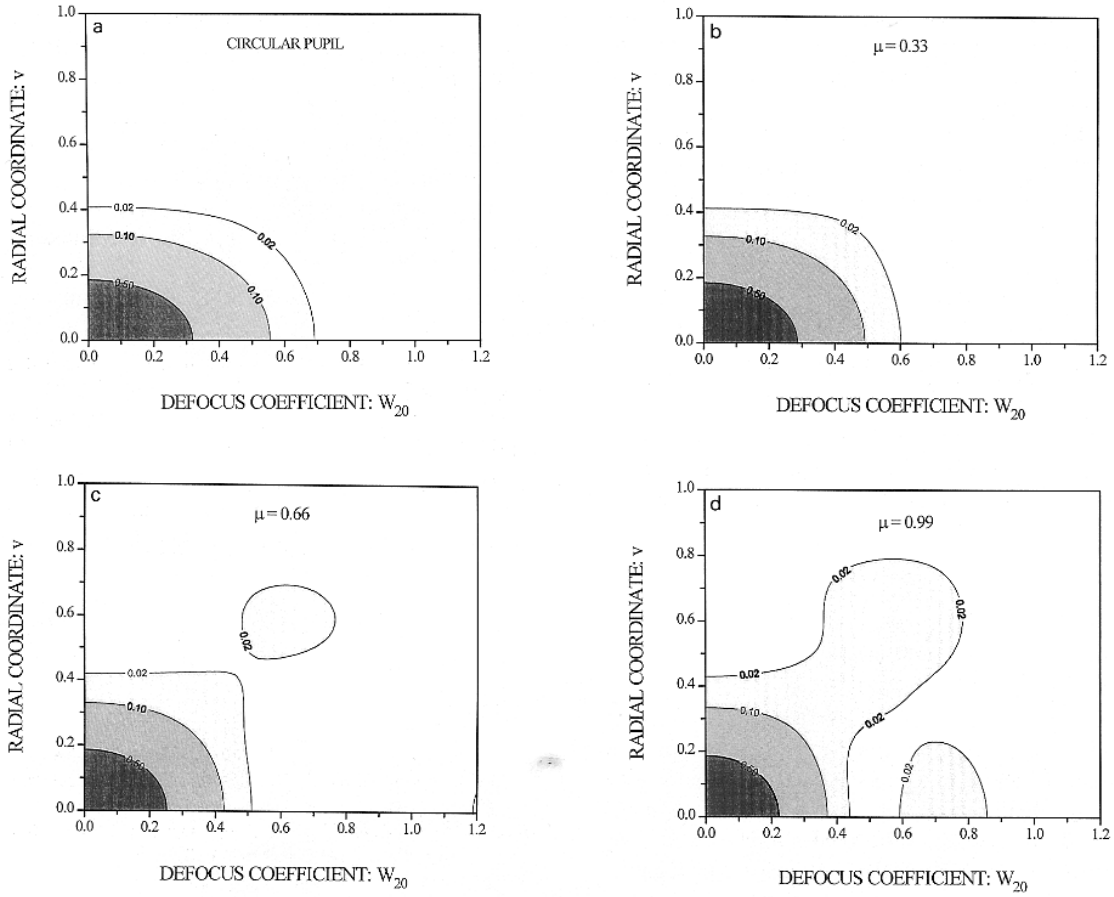

Fig. 6. Theoretical contours of equal normalized intensity (isophotes) in a meridional plane, when the pupil of the collecting system is: (a) unapodized; (b) apodized with the binary filter of $\mu=0.33$; (c) apodized with the binary filter of $\mu=0.66$; and (d) apodized with the binary filter of $\mu=0.99$.

cular aperture, $p_1(0, W_{20})$. This effect is quite apparent when comparing Fig. 5 with Fig. 2.

Furthermore, as it was noted in Section 3, the central lobe of the transverse PSF of an optical system does not spread when the pupil of the system is apodized with one of our filters. Then, it follows that the transverse PSF of a confocal system remains unaffected when, for instance, the collecting-system pupil is apodized with one of these binary filters. Thus, we can conclude that the volume of the central lobe of the 3D PSF of the confocal system is highly reduced, as it is clearly shown by the isophote diagrams of Fig. 6. This fact is of great importance in confocal microscopy because it permits to increase the sectioning properties of such systems, while keeping their transverse resolution capacity.

Finally, due to the special nature of the confocal microscope architecture, the loss of energy produced by the interposition of an annular obstruction in the collecting-system pupil was no relevant importance because in such systems the source power can be arbitrarily modified, between certain limits.

5. Conclusions

We have designed a new set of annular binary filters, which have the ability of tuning the axial resolution of an imaging formation system, simply by changing the

value of the obscuration-ratio parameter μ. We have also pointed out that the use of these filters does not affect, up to the second-order approximation, the transverse resolution of the system.

Finally, we have recognized that when these filters are applied for apodizing a confocal microscope it is possible to obtain a drastic reduction of the area of the central lobe of the 3D PSF. This 3D superresolution effect is of great importance for improving the quality of the image.

Acknowledgements

This work was supported by the Dirección General de Investigación Científica y Técnica (grant PB93-0354-CO2-01), Ministerio de Educación y Ciencia, Spain.

Appendix

The kernel of the Fourier transform in Eq. (4) can be expanded as a power series as

$$\exp(-i2\pi W_{20}\zeta) = \sum_{n=0}^{\infty} \frac{(-i2\pi W_{20}\zeta)^n}{n!} . \tag{A.1}$$

Then, Eq. (4) can be rewritten in terms of the different moments, m_n, of the function $q(\zeta)$ as

$$p(0, W_{20}) = \sum_{n=0}^{\infty} \frac{(-i2\pi W_{20})^n}{n!} m_n . \tag{A.2}$$

Now, for small distances from the paraxial focus, and assuming that the pupil function is real, the axial intensity PSF can be written as

$$\begin{aligned} I(0, W_{20}) &= |p(0, W_{20})|^2 \\ &\approx m_0^2 + 4\pi^2 (m_1^2 - m_0 m_2) W_{20}^2 . \end{aligned} \tag{A.3}$$

Finally, dividing Eq. (A.3) by $I(0, 0)$ we obtain that the normalized axial intensity varies in the form

$$\begin{aligned} I_N(0, W_{20}) &= \frac{I(0, W_{20})}{I(0, 0)} \\ &= 1 + 4\pi^2 \left[\left(\frac{m_1}{m_0} \right)^2 - \frac{m_2}{m_0} \right] W_{20}^2 \\ &= 1 - 4\pi^2 \sigma^2 W_{20}^2 . \end{aligned} \tag{A.4}$$

For the case of the transverse PSF, we use the formula of the power expansion of the zero-order Bessel function [24], i.e.,

$$J_0(2\pi v\sqrt{\zeta + 0.5}) = \sum_{n=0}^{\infty} \frac{(-1)^n}{(n!)^2} (\pi v\sqrt{\zeta + 0.5})^{2n} . \tag{A.5}$$

Then, Eq. (6) can be rewritten in terms of the moments of $q(\zeta)$ as

$$p(v, 0) = m_0 + \pi^2 (m_0/2 + m_1) v^2 + \cdots . \tag{A.6}$$

So, the transverse intensity PSF, up to the second-order approximation, is

$$I(v, 0) = m_0^2 - \pi^2 (m_0^2 - 2m_0 m_1) v^2 , \tag{A.7}$$

whose normalized version reads

$$\begin{aligned} I_N(v, 0) &= \frac{I(v, 0)}{I(0, 0)} = 1 - \pi^2 \left(1 + 2\frac{m_1}{m_0} \right) v^2 \\ &= 1 - \pi^2 (1 + 2\bar{\zeta}) v^2 . \end{aligned} \tag{A.8}$$

References

[1] P. Jacquinot and B. Rozien-Dossier, Apodisation, in: Progress in optics, Vol. III, ed. E. Wolf (North-Holland, Amsterdam, 1964).
[2] C.S. Chung and H.H. Hopkins, J. Mod. Optics 35 (1988) 1485.
[3] G.R. Boyer, Appl. Optics 15 (1976) 587.
[4] B.R. Frieden, Opt. Acta 16 (1969) 795.
[5] J. Ojeda-Castañeda and L.R. Berriel-Valdós, Optics Lett. 13 (1988) 183.
[6] J. Ojeda-Castañeda, J.C. Escalera, and M.J. Yzuel, Optics Comm. 114 (1995) 189.
[7] J. Ojeda-Castañeda, P. Andrés and A. Díaz, J. Opt. Soc. Am. A 5 (1988) 1233.
[8] J. Ojeda-Castañeda, P. Andrés and M. Martínez-Corral, Appl. Optics 31 (1992) 4600.
[9] M. Martínez-Corral, P. Andrés and J. Ojeda-Castañeda, Appl. Optics 33 (1994) 2223.
[10] J. Tsujiuchi, Correction of optical images by compensation of aberrations by spatial frequency filtering, in: Progress in optics, Vol. II, ed. E. Wolf (North-Holland, Amsterdam, 1963).
[11] C.J.R. Sheppard and Z.S. Hegedus, J. Opt. Soc. Am. A 5 (1988) 643.
[12] Z.S. Hegedus, Opt. Acta 32 (1985) 815.
[13] Z.S. Hegedus and V. Sarafis, J. Opt. Soc. Am. A 3 (1986) 1892.
[14] I.J. Cox and C.J.R. Sheppard, J. Opt. Soc. Am. A 3 (1986) 1152.
[15] T. Wilson and S.J. Hewlett, J. Mod. Optics 37 (1990) 2025.
[16] C.J.R. Sheppard and M. Gu, Optics Comm. 84 (1991) 7.

[17] J. Grochmalicki, E.R. Pike, J.G. Walker, M. Bertero, P. Boccacci and R.E. Davies, J. Opt. Soc. Am. A 10 (1993) 1074.
[18] S.W. Hell, S. Lindik and E.H.K. Stelzer, J. Mod. Optics 41 (1994) 675.
[19] M.J. Yzuel, J.C. Escalera and J. Campos, Appl. Optics 29 (1990) 1631.
[20] S. Weissbach and F. Wyrowski, Appl. Optics 31 (1992) 2518.
[21] M. Kowalczyk, M. Martínez-Corral, T. Cichocki and P. Andrés, Optics Comm. 14 (1995) 211.
[22] T. Wilson, ed., Confocal microscopy (Academic, London, 1990).
[23] C.J.R. Sheppard and A. Choudhury, Opt. Acta 24 (1977) 1051.
[24] M. Abramowitz and I.A. Stegun, eds., Handbook of mathematical functions (Dover, New York, 1970).